
Prediction of friction development during transient diesel engine operation using a detailed model

C.D. Rakopoulos* and E.G. Giakoumis

Internal Combustion Engines Laboratory,
Thermal Engineering Department,
School of Mechanical Engineering,
National Technical University of Athens,
9 Heron Polytechniou Str.,
Zografou Campus, 15780 Athens, Greece
E-mail: cdrakops@central.ntua.gr E-mail: vgiakms@central.ntua.gr

*Corresponding author

Abstract: An experimentally validated simulation code is used to study the development and contribution of various friction components during turbocharged diesel engine transients. This is accomplished with the use of a recently proposed detailed friction model. Mean friction mean effective pressure modelling is found to considerably underestimate actual friction around firing TDC, leading to lower speed droops for abrupt load increases. The piston rings assembly contribution is dominant for the particular engine, due to its high number of piston rings and its low crankshaft speed. The model can be used to investigate such interesting cases as the effect of engine oil temperature on engine transient response, or the variation of oil film thickness during a cycle or a transient event.

Keywords: bearings; friction; friction mean effective pressure; oil temperature; piston rings; transient operation; turbocharged diesel engine; valve train.

Reference to this paper should be made as follows: Rakopoulos, C.D. and Giakoumis, E.G. (2007) 'Prediction of friction development during transient diesel engine operation using a detailed model', *Int. J. Vehicle Design*, Vol. 44, Nos. 1/2, pp.143–166.

Biographical notes: Constantine D. Rakopoulos is Head of the Thermal Engineering Department, Full Professor of Internal Combustion Engines and Director of I.C. Engines Laboratory at the School of Mechanical Engineering of the National Technical University of Athens (NTUA), Greece. He graduated (Dipl.Ing.) from the NTUA (Greece) and obtained his MSc, DIC and PhD Degrees from Imperial College London, UK. He has been responsible for the development of engines research at the School of Mechanical Engineering of the NTUA for the last 25 years, with over 130 refereed-papers in International journals and conferences.

Evangelos G. Giakoumis is Dipl.Ing. and Dr.Ing. from the School of Mechanical Engineering of the National Technical University of Athens (NTUA), Greece. He has worked for six years as Area Manager at the After-Sales Department of the Peugeot Automobiles Distributor in Greece, and has been recently appointed Lecturer at the Thermal Engineering Department of the School of Mechanical Engineering of the NTUA. His research interests include diesel engine experimental and simulation analysis under transient conditions, and second-law analysis of internal combustion engines.

1 Introduction

The turbocharged compression ignition (diesel) engine is nowadays the most preferred prime mover in medium and medium-large units applications (truck driving, land traction, ship propulsion, electrical generation), due to its reliability that is combined with excellent fuel efficiency. Nonetheless, its transient operation is often linked with off-design (e.g., turbocharger lag) and consequently non-optimum performance. This leads to unacceptable exhaust emissions and poor speed response, and on the other hand, points out the significance of proper interconnection between the various engine components (governor, fuel pump, turbocharger and load).

During the last decades, diesel engine modelling and experimental investigation has paved the way for an in-depth study of transient operation. These works have dealt, among other things, with fundamental or parametric study (Winterbone et al., 1976; Watson and Marzouk, 1977; Watson, 1981; Winterbone, 1986; Rakopoulos and Giakoumis, 1998), effect of governor design (Rakopoulos et al., 1997), second-law analysis (Rakopoulos and Giakoumis, 2004), experimental study of emissions (Arcoumanis et al., 1994), starting (Gardner and Henein, 1988) etc.

Friction torque varies significantly during the 720 degrees crank angle of a four-stroke engine cycle (Heywood, 1988; Richardson, 2000). Its magnitude compared to the brake torque is not negligible, particularly at low loads where the most demanding transient events commence. Its modelling is, however, difficult due to the interchanging character of lubrication (boundary, mixed, hydrodynamic) and the large number of components involved, i.e., piston rings, piston skirt, loaded bearings, valve train and auxiliaries that cannot be easily isolated, experimentally investigated, and studied separately even at steady-state conditions (Gish et al., 1958; McGeehan, 1978; Richardson, 2000). Moreover, during transient operation, friction is characterised by non steady-state behaviour, differentiating engine response and performance when compared to the corresponding steady-state values, at the same engine speed and fuelling conditions. Winterbone and Tennant (1981) assumed that friction torque should be overestimated during the transient event by some percentage, to account for the peculiarities of transient operation. This aspect has also been investigated by Rakopoulos et al. (2004a), where the transient friction torque was increased in relation to the instantaneous crankshaft deceleration.

Strangely, friction modelling in transient simulation codes has almost always in the past been used in the form of *mean fmep* relations (the works by Keribar and Morel (1987), Gardner and Henein (1988) and by Tuccilo et al. (1993) being three notable exceptions), remaining constant for every degree crank angle in each cycle in the model simulation. This is due to the scarcity-complexity of detailed friction simulations, but it may also be attributed to the fact that friction modelling does not affect heat release rate but only the crankshaft energy balance; the latter one being, nonetheless, essential for correct transient predictions. Consequently, correct friction modelling does not diversify the *interior* engine indicating properties and thus exhaust emissions. However, by defining engine losses magnitude, it directly affects brake specific fuel consumption that is of paramount importance to the engine designer.

The sensitivity of transient operation predictions to friction modelling errors was investigated by Watson (1981). He showed that a 50% overestimation in friction torque could lead to an almost equal increase in predicted final engine speed droop. He also proposed application of the mean fimep equation at each computational step rather than each cycle.

Tuccilo et al. (1993) gave some preliminary transient results incorporating the Rezeká–Henein friction model, thus confirming the importance of analytical friction modelling on transient predictions. Rakopoulos et al. (2004a) incorporated the Rezeká–Henein model in a transient simulation code too, and showed that mean fimep modelling could underestimate engine speed response by up to 12%.

In this work, the more fundamental model proposed by Taraza et al. (2000) is adopted to analytically simulate each friction component. This model separates friction torque into four terms allowing for detailed modelling at each degree crank angle, in contrast to the mean fimep approach where friction torque remains steady over the 720 degrees crank angle of each four-stroke engine cycle. By so doing, we will be able to estimate the contribution of each friction component during a cycle and over a transient event. This is believed to contribute to more accurate transient simulations. Moreover, the development and effect of such interesting parameters as the oil film thickness or the engine oil temperature can be studied.

A transient diesel engine model has been developed and validated by the present research group, which incorporates some important features to account for the peculiarities of the transient operations. Improved relations concerning fuel injection, combustion, dynamic analysis, heat transfer to the cylinder walls, and turbocharger with aftercooler operation during transient response have been developed, which contribute to an in-depth modelling (Rakopoulos et al., 1997; Rakopoulos and Giakoumis, 1998, 2004).

The analysis carried out will be given in a series of diagrams, which depict speed as well as other interesting engine variables response such as fuel pump rack position or boost pressure. Owing to the narrow speed range of the engine in hand, mainly load increases under constant governor setting are investigated, which, nonetheless, play a significant role in the European Transient Cycles of heavy duty vehicles. The contribution and development of each friction component during steady-state and transient operation will be studied and discussed, as well as the variation of oil film thickness, and the effect of operating parameters such as the applied load or speed increases or the engine oil temperature.

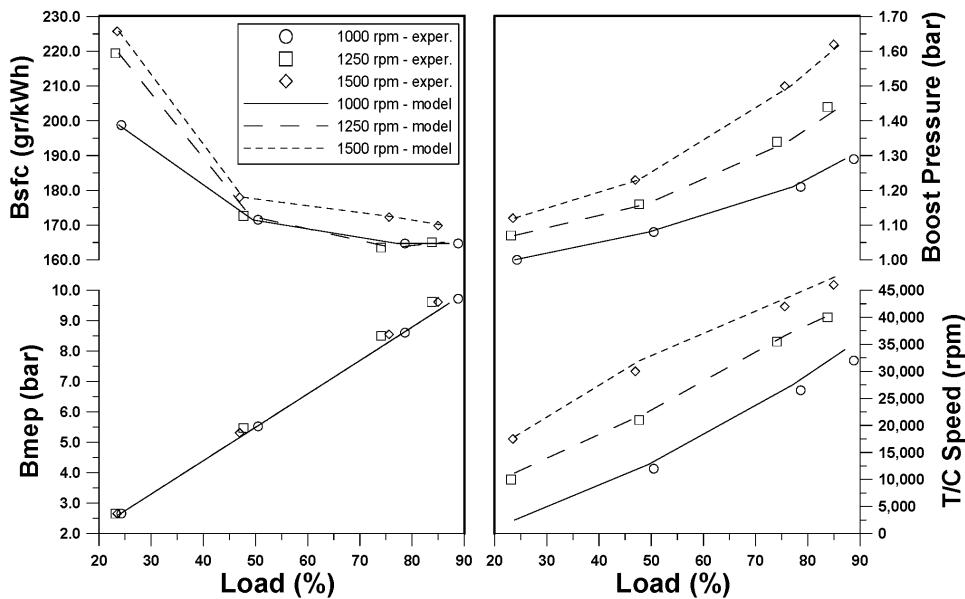
2 Experimental study

The experimental investigation was conducted on a heavy-duty, six-cylinder, turbocharged and aftercooled, medium-high speed diesel engine. The basic data for the engine and turbocharger are given in Table 1.

The first requirement from the engine test bed instrumentation was to investigate the steady-state performance of the engine in question. The matching between experimental and predicted steady-state results is given in Figure 1. This is seen to be rather successful for the whole engine operating range, with the same set of sub-models constants.

Table 1 Basic data for the engine and turbocharger

Engine model and type	MWM TbRHS 518S In-line, six-cylinder, four-stroke, compression ignition, turbocharged, aftercooled, heavy-duty
Speed range	1000–1500 rpm
Bore/stroke/swept volume	140 mm/180 mm/2.77 lt per cylinder
Compression ratio	17.7 : 1
Maximum power	320 HP (236 kW)@1500 rpm
Maximum torque	1520 Nm@1250 rpm
Fuel pump	Bosch PE-P series, in-line, 6-cylinder with mechanical governor Bosch RSUV 300/900
Turbocharger	KKK M4B 754/345 Single-stage, centrifugal compressor, Single-stage, twin entry, axial turbine
Moment of inertia	Engine and brake: 15.60 kg m ² Turbocharger: 7.5 × 10 ⁻⁴ kg m ²

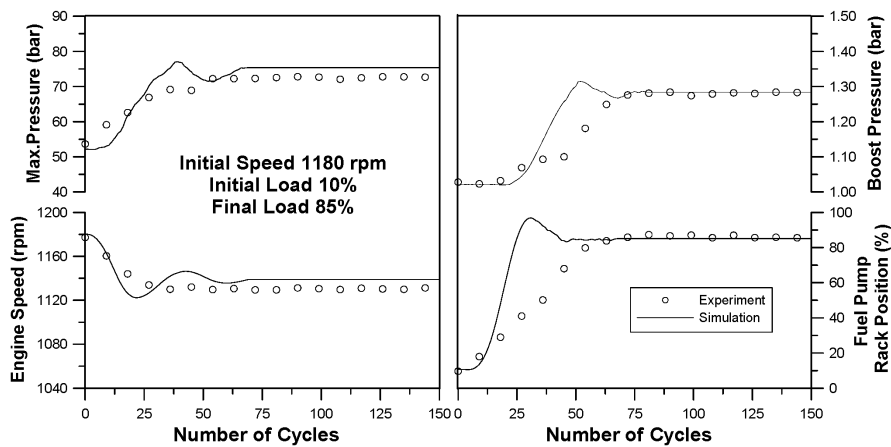
Figure 1 Experimental and predicted steady-state results over the whole engine operating range

Since the particular engine is one with a relatively small speed range, mainly load changes (increases) with constant governor setting were examined. For the transient tests conducted, the initial speed was 1180 or 1380 rpm and the initial load 10% of the engine full load. The final conditions for the transient events varied from 47 to 95% of the engine full load.

A typical example of a conducted transient experiment is given in Figure 2, showing the response of some important first-law properties. Here, the initial load was 10% of the full engine load at 1180 rpm. The final load applied was almost 85% of the full engine

load. The application of the final load was effected by the movement of the brake control lever, which in turn increased the amount of water inside the brake by appropriately increasing the active surface of the inlet tube. However, this hydraulic brake is characterised by a high mass moment of inertia, in the order of 5.375 kg m^2 , resulting in long and *non-linear* actual load-change times and profile. The overall matching between experimental and predicted transient responses is satisfactory for all final values of the engine and turbocharger variables. The fuel pump rack position is notably delayed compared to the speed profile due to the hysteresis induced by the governor. Boost pressure and, mainly, main chamber maximum pressure are closely correlated to the fuel pump rack position response.

Figure 2 Experimental and predicted engine transient response to an increase in load



3 Simulation analysis

3.1 General process description

Since the present analysis does not include prediction of exhaust emissions and on the other hand deals with transient operation calculations on a degree CA basis, a single-zone model is used as the basis for thermodynamic processes evaluation. This approach combines satisfactory accuracy with limited PC program execution time. Polynomial expressions from Heywood (1988), with a 298 K reference datum, are used for each of the four species (O_2 , N_2 , CO_2 , and H_2O) considered. They concern evaluation of internal energy and specific heat capacities for first-law application to the cylinder contents, using the filling and emptying modelling technique on a degree crank angle basis (Winterbone, 1986; Heywood, 1988; Rakopoulos and Giakoumis, 1998; Rakopoulos et al., 2004b).

3.2 In-cylinder processes

For heat release rate predictions, the fundamental model proposed by Whitehouse and Way (1969–1970) is used. In this model the combustion process consists of two parts, i.e., a preparation limited and a reaction limited (Arrhenius type) combustion rate.

It is vital for a proper simulation of transient response that combustion modelling takes into consideration the continuously changing nature of operating conditions. Thus constant K , in the (dominant) preparation rate equation of the Whitehouse–Way model, is correlated with the Sauter mean diameter (SMD) of the fuel droplets through a formula of the type $K \propto (1/\text{SMD})^c$ (Benson and Whitehouse, 1979).

The improved model of Annand and Ma (1970–1971) is used to simulate heat loss Q_L to the cylinder walls,

$$\frac{dQ_L}{dt} = A \left\{ \frac{k_g}{D} \text{Re}^b \left[a(T_g - T_w) + \frac{a'}{\omega} \frac{dT_g}{dt} \right] + c(T_g^4 - T_w^4) \right\}. \quad (1)$$

where a , a' , b and c are constants evaluated after experimental matching at steady-state conditions, k_g is the gas thermal conductivity (W/m K), and the Reynolds number Re is calculated with a characteristic speed derived from a k - ε turbulence model and a characteristic length equal to the piston diameter.

During transient operation, the thermal inertia of the cylinder wall is taken into account using a detailed heat transfer scheme, which models the temperature distribution from the gas to the cylinder wall up to the coolant (convection from gas to internal wall surface and from external wall surface to coolant, and conduction across the cylinder wall).

3.3 Engine dynamics

If G_{tot} represents total system moment of inertia (engine, flywheel and load), then the conservation of energy principle applied to the total system (engine plus load) yields:

$$\tau_e(\varphi, \omega) - \tau_{fr}(\varphi, \omega)_{\text{trans}} - \tau_{\text{Load}}(\omega) = G_{\text{tot}} \frac{d\omega}{dt}. \quad (2)$$

where $\tau_e(\varphi, \omega)$ stands for the instantaneous value of the indicated engine torque, consisting of gas and inertia forces torque.

The connecting rod is modelled as a rigid body experiencing reciprocating and rotating, at the same time, movement (Rakopoulos and Giakoumis, 1998). Also, $\tau_{\text{Load}}(\omega)$ is the load torque, which, for the hydraulic brake coupled to the engine examined, is $\propto \omega^2$. Lastly, $\tau_{fr}(\varphi, \omega)_{\text{trans}}$ stands for the friction torque during transient operation, which will be analysed in detail in Section 4.

3.4 Multi-cylinder model

At steady-state operation the performance of each cylinder is essentially the same, due to the steady-state operation of the governor clutch resulting in the same amount of fuel being injected per cycle. At transient operation, on the contrary, each cylinder experiences different fuelling and air mass flow rates during the same engine cycle due to the continuous movement of the fuel pump rack, initiated by load or speed changes. These differentiations in fuelling and air flow can result in significant differentiations in torque response and finally speed, so affecting significantly the whole engine operation. A multi-cylinder engine model is thus developed, i.e., one in which all the governing differential and algebraic equations are solved individually for every one cylinder of the

six-cylinder engine under study. This ‘multi-cylinder’ approach can offer better results as regards manifolds simulation even at steady-state conditions, since the exhaust manifold is modelled to exchange mass only with that cylinder which experiences exhaust of gases at the particular computational step, while, at the same time, interactions between exhausting cylinders, which can under certain circumstances lead to backflow, are also taken into account.

3.5 Fuel pump operation

A mathematical fuel injection model, experimentally validated at steady-state conditions, is applied to simulate the fuel pump-injector lift mechanism (Rakopoulos and Hountalas, 1996), taking into account the delivery valve and injector needle motion. The unsteady gas flow equations are solved using the method of characteristics, providing the dynamic injection timing as well as the duration and the rate of injection for each cylinder at each transient cycle. The obvious advantage is here that the transient operation of the fuel pump is also taken into account, mainly through the fuel pump residual pressure value, which is built up together with the other variables during the transient event. Moreover, this individual fuel injection ‘subroutine’ is called once for every cylinder at each cycle with the values of angular velocity, fuel pump rack position and pump residual pressure existing at the point of the individual cylinder’s static injection timing.

4 Friction modelling

4.1 Mean fmep method

For the calculation of friction inside the cylinder, we try at first the method used so far by all other researchers in the field, i.e., the *mean fmep* approach. For the engine in hand, we have the following relation for the evaluation of fmep (in bar) (Chen and Flynn, 1965; Ciulli, 1993):

$$\text{fmep} = \alpha + \beta p_{\max} + \gamma \bar{u}_{\text{pist}}, \quad (3)$$

where p_{\max} is the cylinder maximum pressure calculated at the previous engine cycle, \bar{u}_{pist} is the corresponding mean piston speed, and α , β , γ are constants derived after calibration against experimental data at steady-state conditions.

Consequently, friction torque is

$$\tau_{fr}(\varphi) = \bar{\tau}_{fr} = (\text{fmep} \times 10^5) A_{\text{pist}} r / 2\pi, \quad (4)$$

where $A_{\text{pist}} = \pi D^2/4$ is the piston cross section area. This friction torque remains constant at every degree crank angle during a cycle, with its values differentiating only from engine cycle to cycle. The important part here is the $\gamma \bar{u}_{\text{pist}}$ factor, in equation (3), indicating the dominant effect of engine speed on friction torque.

4.2 Analytical method (Taraza et al. model)

Secondly, the method proposed by Taraza et al. (2000) is adopted, which describes the non-steady profile of friction torque during each cycle. Unlike the rather empirical Rezek and Henein (1984) approach, which required the use of many correction coefficients, the Taraza et al. model is based on a fundamental friction analysis. In this method the total amount of friction is divided into four parts, i.e., piston rings assembly (including piston rings and piston skirt contribution), loaded bearings, valve train and auxiliaries. The power cylinder and the valve train contribution were experimentally validated. A brief description of the model will be given in the next subsections. More details can be found in Stanley et al. (1999) and Taraza et al. (2000).

4.2.1 Piston rings assembly

For most of the piston stroke, lubrication is hydrodynamic with metal contact occurring near firing top dead centre (TDC). The duty parameter s of the typical Stribeck diagram (see also Figure 3) is

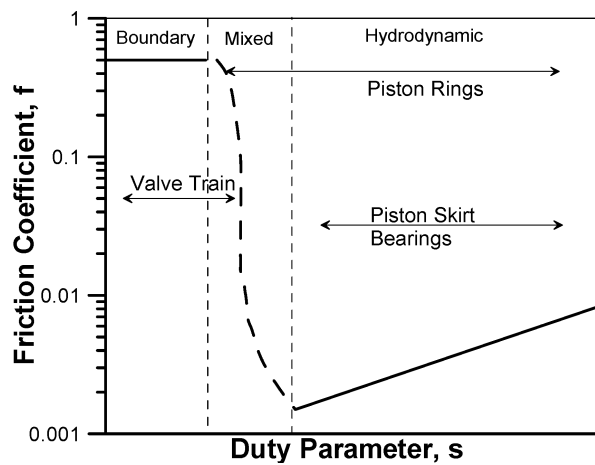
$$s = \frac{\mu_{\text{oil}} |u_{\text{pist}}|}{F_{\text{ring}} / L_{\text{ring}}} \quad (5)$$

with L_{ring} the active length of the ring profile, and u_{pist} the instantaneous piston velocity (Rakopoulos and Giakoumis, 1998)

$$u_{\text{pist}} = r\omega \left[\sin \varphi + \frac{r}{L_{\text{crod}}} \frac{\sin \varphi \cos \varphi}{\sqrt{1 - \left(\frac{r}{L_{\text{crod}}}\right)^2 \sin^2 \varphi}} \right], \quad (6)$$

where r is the crank radius and L_{crod} the connecting rod length.

Figure 3 Stribeck diagram of friction coefficients for various internal combustion engine components



The normal force of the ring profile F_{ring} , which is the sum of the ring diametral elastic tension (T_{DE}) and the instantaneous force from the gas pressure inside the cylinder, is given by

$$F_{\text{ring}} = 2T_{DE} + \pi D w_{\text{ring}} p_g. \quad (7)$$

The oil viscosity μ_{oil} is approximated by Zweiri et al. (2000)

$$\mu_{\text{oil}} = 7.849 \times 10^{-5} \exp\left(\frac{-8.670 \times 10^{-3} T_{\text{oil}}^2 - 1.15311 T_{\text{oil}} + 1361}{T_{\text{oil}} + 133} + \frac{p_{\text{oil}}}{105}\right) \quad (8)$$

with the dominant contribution coming from oil temperature T_{oil} . Generally, a constant (mean) oil film temperature is assumed. Harigaya et al. (2003) conducted a detailed simulation and experimental validation of piston ring oil film thickness variation, for a DI diesel engine, using unsteady two-dimensional energy equation with heat generated from viscous dissipation. They showed that oil film temperature varies during an engine cycle, about 5–10% around its mean value, and so does oil viscosity. For the current analysis, we have tried a polynomial approximation of oil film temperature variation around its mean value, according to the remarks by Harigaya et al. (2003). The resultant differentiation in the obtained transient response of the engine properties was found to be less than 1%.

For hydrodynamic lubrication, the friction coefficient is (McGeehan, 1978; Heywood, 1988; Stanley et al., 1999; Taraza et al., 2000)

$$f_{\text{pr}} = Cs^m \quad (9a)$$

whereas, for the mixed lubrication regime, it is

$$f_{\text{pr}} = f_o \left(1 - \frac{s}{s_{\text{cr}}}\right) + f_{\text{cr}} \frac{s}{s_{\text{cr}}} \quad (9b)$$

with $f_o = 0.28$, $f_{\text{cr}} = 0.0225$ and $s_{\text{cr}} = 0.0001$ for cast iron (Taraza et al., 2000).

The corresponding ring friction force is

$$F_{\text{pr}} = f_{\text{pr}} F_{\text{ring}}. \quad (10)$$

Force F_{pr} is computed separately for each (compression or oil) ring. According to Zweiri et al. (2000), who have recently proposed an interesting analytical friction model too, the diametral elastic force needed in equation (7) can be calculated from geometrical ring data, i.e.,

$$T_{DE} = \frac{2 \times 1.778 E (\pi / 64) w_{\text{ring}}^4 g}{\pi (d_{\text{ring}} / 2 - w_{\text{ring}} / 2)^3} \quad (11)$$

with g the gap closure of each ring and E its material Young modulus of elasticity.

Oil film thickness between ring and cylinder liner can then be calculated from

$$h_{\text{oil}} \cong w_{\text{ring}} s \quad (12)$$

with s the Stribeck duty parameter given by equation (5). An approximation sign is used in equation (12) since at the dead centres, where the piston velocity and hence the duty parameter ' s ' are zero, the oil film thickness ' h_{oil} ' is not zero due to oil squeeze effects.

For the piston skirt similar considerations are made, bearing in mind that lubrication is here always hydrodynamic. The corresponding friction coefficient is (Stanley et al., 1999; Taraza et al., 2000)

$$f_{ps} = C_{ps} \sqrt{\frac{\mu_{oil} |u_{pist}|}{F_{thr} / L_{ps}}} \quad (13)$$

and the respective friction force

$$F_{ps} = f_{ps} F_{thr} \quad (14)$$

where F_{thr} is the thrust force between piston and liner (Rakopoulos and Giakoumis, 1998) and L_{ps} the length of the piston skirt.

Total piston rings assembly friction torque is given by

$$\tau_{pra} = (F_{rings} + F_{ps}) \times r \times \left[\sin \varphi + \frac{r}{L_{crod}} \frac{\sin \varphi \cos \varphi}{\sqrt{1 - \left(\frac{r}{L_{crod}}\right)^2 \sin^2 \varphi}} \right]. \quad (15)$$

Figure 4 shows the development of piston rings assembly friction forces during an engine cycle, for the MWM engine under study. The main data for the engine that are needed for the application of friction equations are provided in Table 2. The profile of piston rings pack and piston skirt friction forces over the 720 degrees crank angle are in accordance with the experimental results provided by Halsband (1994), Stanley et al. (1999), and Richardson (2000), as regards both instantaneous values and overall trends. The piston rings force is determined by the gas pressure variation, assuming its greatest value around firing TDC (negative values denote piston movement towards the BDC), whereas during compression, and inlet and exhaust strokes, its magnitude is much lower. On the other hand, piston skirt development follows closely the instantaneous piston speed as has already been experimentally confirmed (Heywood, 1988; Stanley et al., 1999; Richardson, 2000).

The prediction of oil film thickness variation from equation (12) is provided in the same Figure. Metal contact between rings and cylinder liner is evident around firing TDC. Owing to the considerable decrease of gas pressures during exhaust and inlet strokes, the oil film thickness assumes much greater values after 360 deg. CA.

Figure 4 Variation of piston rings assembly friction force and oil film thickness during an engine cycle for cylinder No. 1

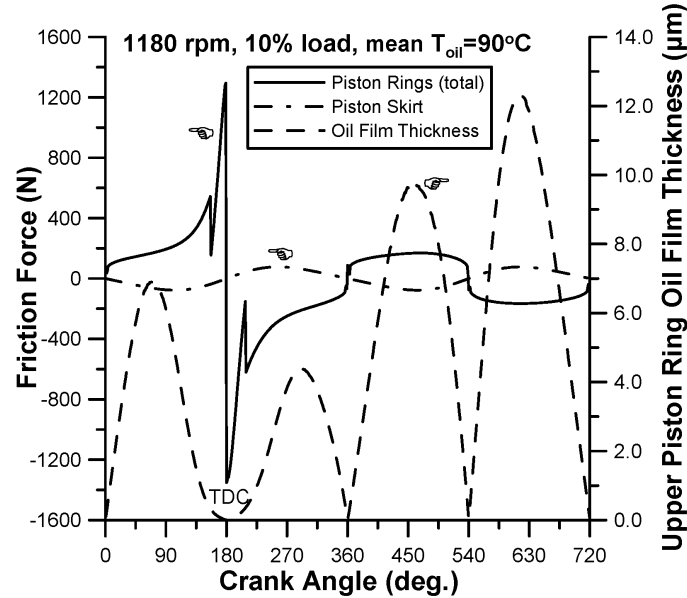


Table 2 Data and constants for the application of mean and analytical friction modelling

Mean fmep method equation (3)	$\alpha/\beta/\gamma : 0.111/0.004/0.1136$
Taraza et al. method equations (5)–(26)	Number of compression rings = 3 Number of oil rings = 2 Compression ring width, $w_c = 3.5$ mm Oil ring width, $w_o = 6$ mm Length of piston skirt, $L_{ps} = 152.5$ mm Journal bearing radius, $r_{jb} = 57.5$ mm Journal bearing radial clearance, $c_{jb} = 0.135$ mm Journal bearing length, $L_{jb} = 52$ mm Con. rod big end bearing radius, $r_{crod} = 49.8$ mm Con. rod big end bearing radial clearance, $c_{crod} = 0.135$ mm Con. rod big end bearing length, $L_{crod} = 62.0$ mm Valve spring preloading force, $F_o = 360$ N Spring stiffness, $K_s = 25,000$ N/m Mean oil temperature, $T_{oil} = 90^\circ\text{C}$ Crank radius, $r = 90$ mm Maximum valve lift, $L_v = 12.5$ mm Arm ratio, $A_R = 1$ Cam width, $L_{cam} = 33$ mm Radius of cam basic circle, $R_{bc} = 30$ mm

4.2.2 Loaded bearings

Friction in bearings is mainly hydrodynamic with the deformation of the bearing housing, due to the applied loading playing an important role. The bearing friction force is computed by the following equation (Taraza et al., 2000)

$$F_{\text{bear}} = \frac{2\pi\mu_{\text{oil}}r_b^2\omega L_b}{c_b\sqrt{1-f^2}} + \frac{eL_F}{2r_b} \sin \varphi, \quad (16)$$

where r_b is the bearing radius, e_b the eccentricity, c_b the radial clearance, L_b the length of the bearing, $f = e_b/c_b$, and L_F the bearing load.

For a constant loaded bearing, friction force will correspond to the short bearing theory, where it holds (Taraza et al., 2000)

$$\frac{L_F/L_b}{r_b\omega\mu_{\text{oil}}}\left(\frac{c_b}{r_b}\right)^2\left(\frac{2r_b}{L_b}\right)^2 = \frac{\pi f}{(1-f^2)^2}\sqrt{0.62^2+1}. \quad (17)$$

For the loading L_F of the bearing, an analysis of the forces-kinematic mechanism of the piston-connecting rod is required, as for example the one by Rakopoulos and Giakoumis (1998).

The above analysis is carried out twice, one for the connecting rod big end bearings and one for the journal bearings. An iterative method is also required in order to solve equation (17), which will provide the value of eccentricity ratio f needed in equation (16).

The respective bearing friction torque is then

$$\tau_b = F_b r_b. \quad (18)$$

4.2.3 Valve train

Valve train friction is governed by friction between cam and tappet and is mainly elasto-hydrodynamic. Valve friction force is given by Taraza et al. (2000)

$$F_{\text{valve}} = 0.11F_{\text{cam}}(1-\lambda) \quad (19)$$

for $\lambda < 1$ (boundary lubrication), while for $\lambda > 1$ (elasto-hydrodynamic lubrication)

$$F_{\text{valve}} = \frac{2b\mu_{\text{oil}}L_{\text{cam}}}{h_{\text{oil}}}, \quad (20)$$

where L_{cam} is the length of the cam and b the half width of the Hertzian line contact.

Force F_{cam} between cam and tappet is given by

$$F_{\text{cam}} = \left(F_o + K_s \frac{L_{\text{valve}}}{2} \right) A_R + m_{\text{cam}} \alpha_{\text{tip}} \quad (21)$$

with F_o the preloading force of the valve spring, K_s its stiffness, L_{valve} the instantaneous valve lift, A_R the arm ratio of the rocker arm, m_{cam} the mass of the cam and α_{tip} the acceleration of the tappet at the tip of the cam.

The actual oil film thickness needed in equation (20) is given by

$$h_{\text{oil}} = 2.65 \left(\frac{\mu_{\text{oil}} u_{\text{cam}}}{2Er_{\text{cam}}} \right)^{0.7} (2.2 \times 10^{-8} E)^{0.54} \left(\frac{F_{\text{cam}} / L_{\text{cam}}}{Er_{\text{cam}}} \right)^{-0.13} r_{\text{cam}} \quad (22)$$

with E the Young's modulus of elasticity of the cam and tappet, $u_{\text{cam}} = r_{\text{cam}} \omega_{\text{cam}}$ the average relative speed between cam and tappet, and r_{cam} the average cam radius based on the radius of the cam basic circle, r_{bc} ,

$$r_{\text{cam}} = r_{\text{bc}} + 0.5 A_R L_{\text{valve}}. \quad (23)$$

Finally, the value of λ for equations (19) is computed from

$$\lambda = h_{\text{oil}} r_{\text{cam}} / \sigma \quad (24)$$

with σ the combined roughness of the cam and tappet surfaces.

The corresponding friction torque is then

$$\tau_{\text{valve}} = F_{\text{valve}} r_{\text{cam}}. \quad (25)$$

Figure 5 depicts the above three described friction contributors for one cylinder of the engine under study, at the initial operating point of the transient event, i.e., engine speed 1180 rpm and 10% load. The contribution of the piston rings term is dominant (almost 70% of the total one), especially during the closed part of the cycle (note the logarithmic scale of the friction torque axis). This term is correlated with the gas pressure p_g , so it is expected to acquire even higher instantaneous values for greater loads. Piston rings contribution assumes such great values due to the large number of rings (five in all) and the increased oil ring width (6 mm). The simulation revealed that a 20% reduction in total friction torque could be accomplished with a reduction in oil ring width from 6 to 4 mm. A further 10% reduction is experienced if the number of rings is reduced from 5 to 3. By so doing the contribution of piston rings assembly on the total friction torque would be 45–50%, which is the typical value reported in the literature (Heywood, 1988; Richardson, 2000).

The effect of the valve train in Figure 5 is evident during the opening of intake and exhaust valves (first term on the right-hand side of equation (21)). The low engine speed significantly limits the contribution of bearings, valves and auxiliaries. The latter will be analysed in the next subsection.

The same friction components variation, based now on the Rezeko and Henein (1984) empirical friction model, is also provided in Figure 6 for comparison (from Rakopoulos et al., 2004a).

4.2.4 Auxiliaries

The Taraza et al. (2000) model covers the auxiliaries terms too, i.e., fuel injection pump, water pump, oil pump, etc., providing equations for the determination of each pump term.

The fuel injection pump contribution consists of two terms, the one term dealing with the operation of the low-pressure fuel pump and the other accounting for the spike during injection

$$\tau_{\text{fpump}}(\varphi) = \pi \frac{d_{\text{fp}}^2}{4} S_{\text{fp}} \frac{N_{\text{cyl}} p_{\text{fp}}}{2 \eta_{\text{fp}}} + \frac{p_{\text{inj}} \dot{Q}_{\text{inj}}}{\omega} \sin\left(\frac{2\pi}{\varphi_d} \varphi\right) \quad (26)$$

with d_{fp} , S_{fp} the diameter and stroke of the fuel pump, η_{fp} its efficiency, p_{fp} its pressure, N_{cyl} the number of engine cylinders, and p_{inj} the injector needle opening pressure. Furthermore, \dot{Q}_{inj} is the fuel flow rate during injection, ω the crankshaft angular velocity, φ the instantaneous crank angle and φ_d the duration of injection.

Figure 5 Components friction torque variation during an engine cycle for cylinder No. 1

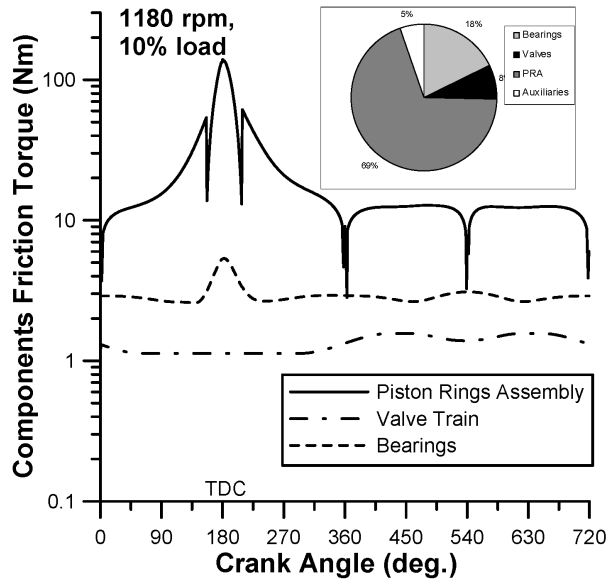
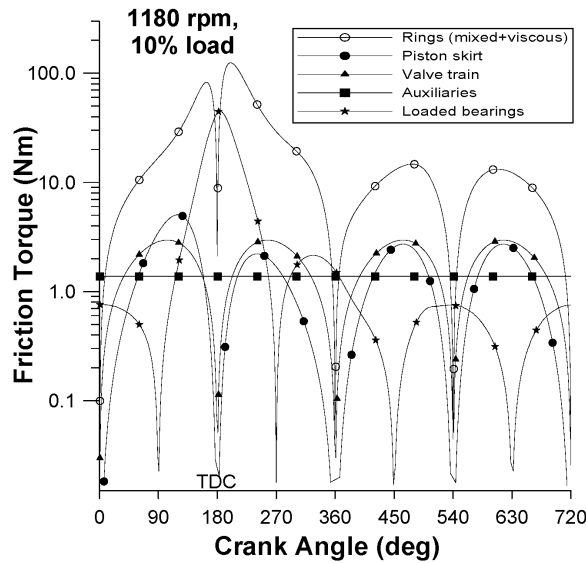


Figure 6 Components friction torque variation during an engine cycle (Rezeka–Henein model) for cylinder No. 1



Similarly, the torque required to drive the oil pump is based on the rate of oil flow in the lubrication system, and the torque required to drive the water cooling pump is calculated from the rate of coolant flow and the pressure in the cooling circuit (Taraza et al., 2000). Total friction torque from auxiliaries is then:

$$\tau_{\text{aux}}(\varphi) = \tau_{\text{fpump}}(\varphi) + \tau_{\text{oilpump}}(\varphi) + \tau_{\text{waterpump}}(\varphi). \quad (26a)$$

4.2.5 Total friction torque

Total friction torque at each degree crank angle is the sum of the above terms (equations (15), (18), (25) and (26a)), i.e.,

$$\tau_{\text{fr}}^{\text{tot}}(\varphi) = \tau_{\text{pra}}(\varphi) + \tau_b(\varphi) + \frac{1}{2}\tau_{\text{valve}}(\varphi) + \tau_{\text{aux}}(\varphi). \quad (27)$$

Despite the increased number of equations needed for application of the detailed friction model, the respective increase in the PC execution time of the simulation code is minimal since, apart from the iterative method of Subsection 4.2.2, all other equations are algebraic; the only real obstacle is here the need for finding a lot of (geometric) data of the engine subsystems.

5 Results during transient operation¹

Figure 7 focuses on the nominal load increase case, with the transient profiles based on both friction models depicted. The two speed curves almost coincide, only until cycle 15. This happens because from cycle 15 onwards the main change in fuelling occurs, a fact leading to differentiations in gas pressure and consequently the profile of friction torque and thus engine speed. The mean fmep curve results differ by 4.5% as regards both maximum and final engine speed droop from the analytical ones. Similar results hold for the boost pressure, which is also depicted in Figure 7, as well as for the engine torque, fuel pump rack position, turbocharger speed etc. In this Figure the case with an oil temperature of 60°C is also depicted, only for the detailed model, since the constant fmep relation does not take into account such operational parameters effect. Lower oil temperature results in increased viscosity (cf. equation (8)) and consequently increased piston rings assembly friction, leading to increased total friction torque and thus greater engine speed droops.

It should be noted here that the particular engine-load configuration has a high total mass moment of inertia, in the order of 15.60 kg m², which when combined with the very small speed range of the engine (1000–1500 rpm), gives slow governor clutch and thus fuel pump rack responses. These in turn lead to relatively slow changes in fuelling.

Figure 8 focuses on the development of the *reduced fmep* term from the Taraza et al. (2000) model, which is identified as follows

$$\text{fmep}_{\text{Taraza}} = \frac{2\pi \int_0^{720} \tau_{\text{fr}}^{\text{tot}}(\varphi)}{A_{\text{pist}}r}. \quad (28)$$

Figure 7 Comparison of response to an increase in load between mean fmep and analytical friction modelling (10–70% load increase, quadratic load-type)

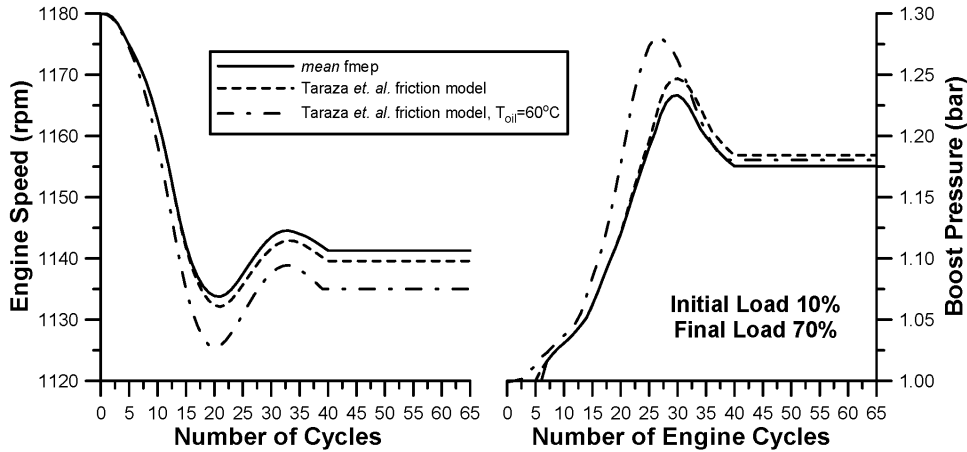
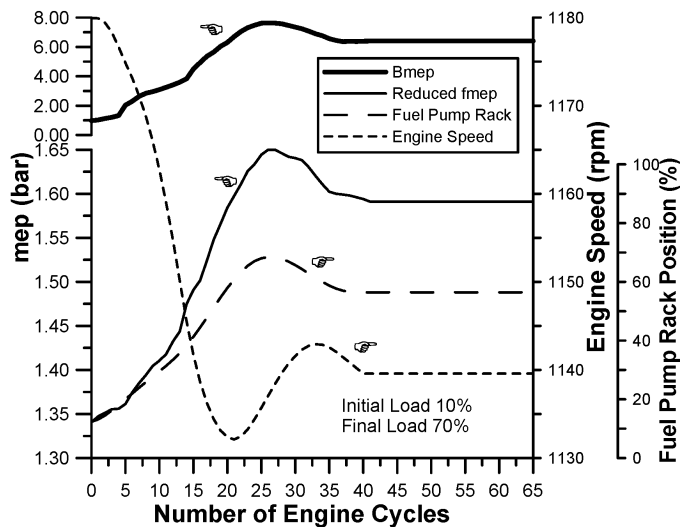


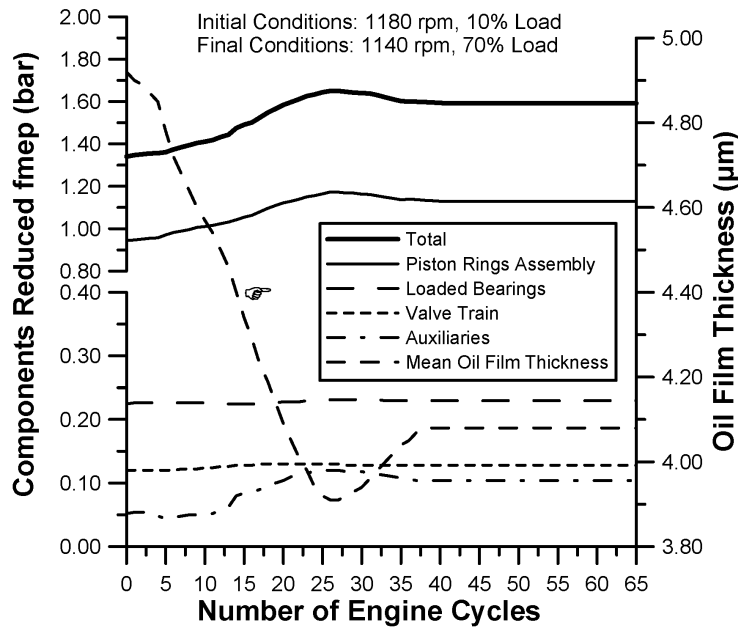
Figure 8 Reduced fmep development vs. engine cycles for the 10–70% load increase



This fmep response arises from the combined result of pressures (through the fuel pump rack position response) and engine speed development. Bmep development for cylinder No. 1 is also provided in this Figure for comparison. Loaded bearings and auxiliaries are mostly dependent on engine speed, with the effect of pressures being dominant for the piston rings assembly. This is best highlighted in Figure 9, which shows the development of the various friction components reduced fmep for the nominal transient load increase of 10–70%. The dominance of the piston rings assembly is obvious (5 piston rings in total, of which the two oil rings having 6 mm width each) with the other terms having smaller contribution to the total fmep, especially at the low engine speed under study. This holds, particularly, for the loaded bearings term, which is heavily dependent on engine speed. Only the friction of auxiliaries is evidently increasing during the transient event due to the significant increase in injected fuel quantity from cycle 15 onwards.

The mean value, over each engine cycle, of the upper piston ring oil film thickness is also provided in the same Figure, with its profile following closely the fuel pump rack position given in Figure 8. The latter defines the level of in-cylinder gas pressures (engine speed varies only modestly during the transient event), which also affect oil film thickness values.

Figure 9 Reduced components fmep and mean oil film thickness vs. engine cycles for the 10–70% load increase



In Figure 10 the variation of total friction torque (equation (27)) during the first and the last cycle of the nominal transient event of 10–70% load increase is given, compared to the mean fmep results of equation (13). The last cycle has a much fuller friction torque diagram, despite the somewhat lower engine speed of 1140 rpm, originating from greater pressures inside the cylinder due to the increased loading. As it is shown, the constant fmep assumption significantly underestimates friction torque for a period of almost 180 degrees CA (around firing TDC), which leads to the smaller speed droops observed in Figure 7. This is better understood in Figure 11, which shows the two predicted engine speed developments during the second half of the first cycle of the transient event, where the load increase commences; the crank angle here corresponds to cylinder No. 1. The increased moment of inertia of the engine-brake set up leads to very large engine non-uniformity and thus limited speed fluctuations. Nonetheless, the greater speed droops of the detailed friction modelling are already apparent.

Figure 12 focuses on the development of oil film thickness prediction for various engine cycles of the transient load increase of 10–70%. As has already been experimentally validated by previous researchers (oil film thickness reducing with increasing in-cylinder gas pressures), we observe a reduction in its values as the transient event develops, for as long as the fuelling increases. This Figure should be studied in conjunction with Figure 8.

Figure 13 investigates the effect of friction modelling adopted, but in this case for a greater load increase of 10–95% and for a linear load-type. Fuel pump rack position and boost pressure response are also depicted for this load change, the load-torque of which is given on the upper-right sub-diagram. Similar remarks hold with those of the previous case, with the mean fmep results differing now by about 6–7% as regards final equilibrium speed. Higher load changes and more demanding load-types lead to more abrupt governor clutch movements and so greater crankshaft angular decelerations, revealing the differentiation in the predictions from the two friction approaches. From Figures 7 and 13 it is revealed that it is actually justified to adopt a detailed, per degree crank angle, friction model for transient operation simulations.

Figure 10 Total friction torque variation at initial and final cycle of the 10–70% load increase, for cylinder No. 1

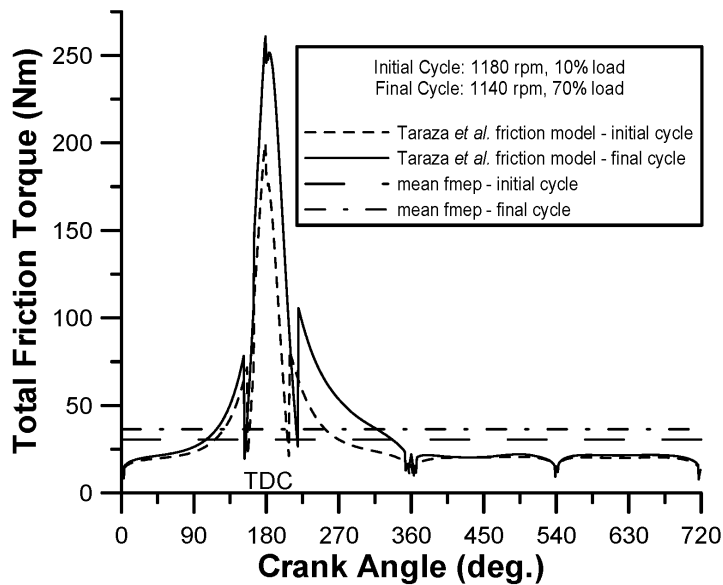


Figure 11 Engine speed development over the second half of the first cycle of the 10–70% load increase

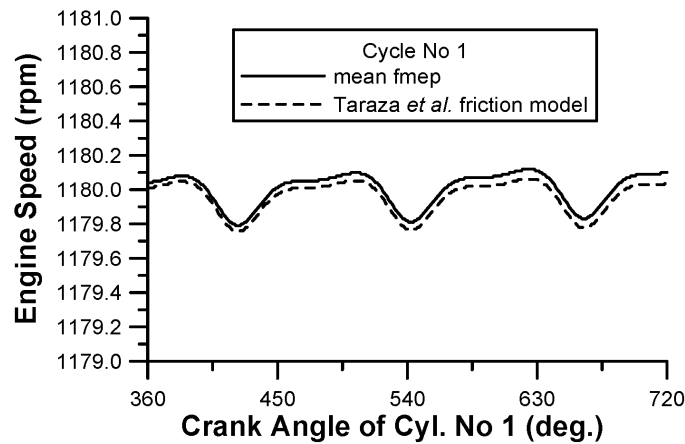


Figure 12 Oil film thickness development over an engine cycle for various cycles of the 10–70% load increase

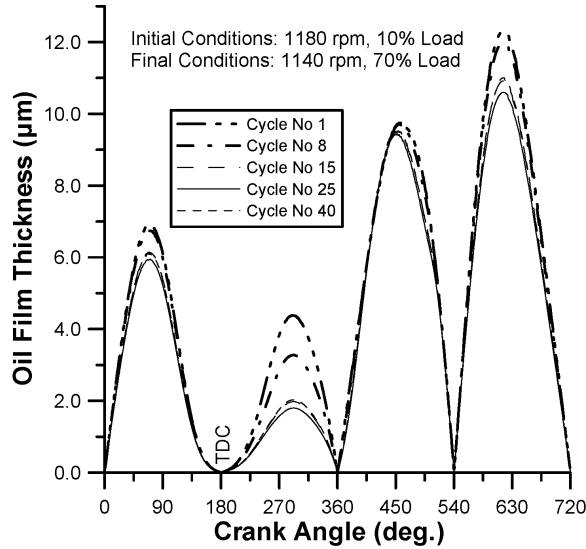
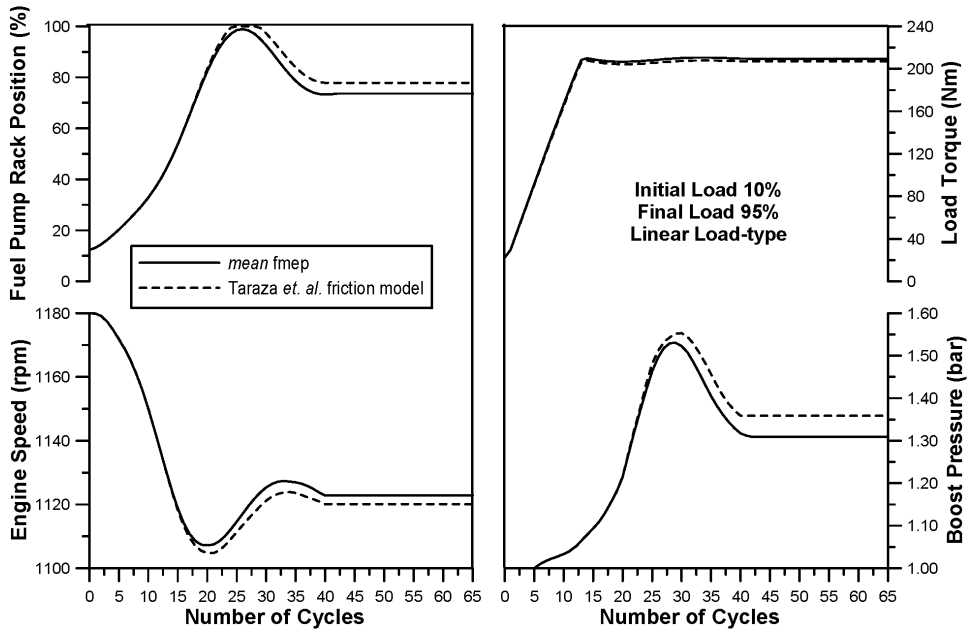


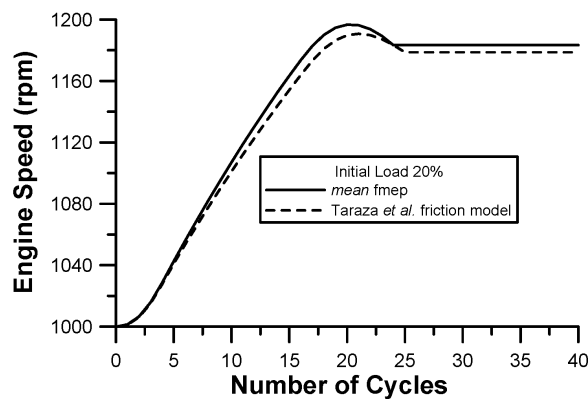
Figure 13 Comparison of response to an increase in load between mean fmep and analytical friction modelling (10–95% load increase, linear load-type)



The difference in the final equilibrium state, for all load schedules examined, implies that there is also a difference in the final fmep values for the two friction models used. Nonetheless, one should not forget that we deal with a dynamic phenomenon that is influenced by many parameters, affecting both its profile and its final equilibrium conditions.

Although the particular engine has a very narrow speed range, we have also investigated the effect of detailed friction modelling as regards speed changes, which is depicted in Figure 14. Again, a distinguishable difference between the two friction modelling approaches exists, in the order of 5–6% even for the very limited speed increase case examined. The mean fmep approach exhibits now greater speed increases, as it was expected from the general remarks made with Figure 10.

Figure 14 Comparison of response to an increase in speed between mean fmep and analytical friction modelling



6 Conclusions

A transient analysis simulation program developed has been used to predict friction torque development and magnitude during transient diesel engine operation, with the use of the fundamental detailed friction equations proposed by Taraza et al. (2000).

- The most significant drawback of the friction model adopted is the need for many input data, which may not always be readily available. On the other hand, the PC burden induced is almost negligible.
- The engine under study had a high mass moment of inertia and a narrow speed range, which did not allow great differences to be revealed. However, differences of 5–7% between the detailed and constant fmep approach have been detected for typical load and speed changes. This, to the authors' mind, justifies the application of the analytical friction modelling for more complete transient simulations.
- It was shown that constant fmep significantly underestimates actual friction torque, mainly around firing TDC, for a period of almost 180 degrees crank angle. This underestimation was reflected in the respective lower values of maximum and final engine speed droops during transients.
- Piston rings assembly contribution is dominant for the present engine, during both steady-state and transient operation, due to the high number of piston rings and the large width of the two oil rings. The overall low crankshaft speed was the main reason for the limited contribution of the loaded bearings.

- Oil film thickness was found to assume almost zero value at firing TDC with its overall values, over an engine cycle during transients, reducing when the fuelling was increased.
- An interesting case with lower engine oil temperature has been investigated too, with the increased friction term leading to greater speed droops compared to the nominal case.

It is the intention of the present research group to proceed to experimental validation in the near future regarding the above mentioned predicted results, at least as regards total friction torque contribution/development during transients.

References

- Annand, W.J.D. and Ma, T.H. (1970–1971) ‘Instantaneous heat transfer rates to the cylinder head surface of a small compression-ignition engine’, *Proc. Inst. Mech. Engrs.*, London, UK, Vol. 185, pp.976–987.
- Arcoumanis, C., Megaritis, A. and Bazari, Z. (1994) ‘Analysis of transient exhaust emissions in a turbocharged vehicle diesel engine’, *Institution of Mechanical Engineers, Conference on Turbocharging and Turbochargers*, Paper C484/038, London, pp.71–81.
- Benson, R.S. and Whitehouse, N.D. (1979) *Internal Combustion Engines*, Pergamon Press, Oxford.
- Chen, S.K. and Flynn, P. (1965) *Development of a Compression Ignition Research Engine*, SAE Paper No. 650733.
- Ciulli, E. (1993) ‘A review of internal combustion engine losses, pt. 2: studies for global evaluations’, *Proc. Inst. Mech. Engrs – Part D: Journal of Automobile Engineering*, London, UK, Vol. 207, pp.229–240.
- Gish, R.E., McCullough, J.D., Retzlaff, J.B. and Mueller, H.T. (1958) ‘Determination of true engine friction’, *Trans. SAE*, Vol. 66, pp.649–661.
- Halsband, M. (1994) ‘Messung und optimierung der reibungsverluste der kolbengruppe – teil 1’, *Motor-Technische Zeitschrift*, Vol. 55, pp.664–671.
- Harigaya, Y., Suzuki, M. and Takiguchi, M. (2003) ‘Analysis of oil film thickness on a piston ring in diesel engine: effect of oil film temperature’, *Trans. ASME, J. of Engineering for Gas Turbines and Power*, Vol. 125, pp.596–603.
- Heywood, J.B. (1988) *Internal Combustion Engine Fundamentals*, McGraw-Hill, New York.
- Gardner, T.P. and Henein, N. (1988) *Diesel Starting: a Mathematical Model*, SAE Paper No. 880426.
- Keribar, R. and Morel, T. (1987) *Thermal Shock Calculations in I.C. Engines*, SAE Paper No. 870162.
- McGeehan, J.A. (1978) *Literature Review of the Effects of Piston Ring Friction and Lubricating Oil Viscosity on Fuel Economy*, SAE Paper No. 780673.
- Rakopoulos, C.D. and Giakoumis, E.G. (1998) ‘Simulation and analysis of a naturally aspirated IDI diesel engine under transient conditions comprising the effect of various dynamic and thermodynamic parameters’, *Energy Conversion and Management*, Vol. 39, pp.465–484.
- Rakopoulos, C.D. and Giakoumis, E.G. (2004) ‘Availability analysis of a turbocharged diesel engine operating under transient load conditions’, *Energy*, Vol. 29, pp.1085–1104.
- Rakopoulos, C.D. and Hountalas, D.T. (1996) ‘A simulation analysis of a DI diesel engine fuel injection system fitted with a constant pressure valve’, *Energy Conversion and Management*, Vol. 37, pp.135–150.

- Rakopoulos, C.D., Giakoumis, E.G. and Hountalas, D.T. (1997) *A Simulation Analysis of the Effect of Governor Technical Characteristics and Type on the Transient Performance of a Naturally Aspirated IDI Diesel Engine*, SAE Paper No. 970633. Also, *Trans. SAE, J. of Engines*, Vol. 106, pp.905–922.
- Rakopoulos, C.D., Giakoumis, E.G. and Rakopoulos, D.C. (2004a) *The Effect of Friction Modelling on the Prediction of Turbocharged Diesel Engine Transient Operation*, SAE Paper No. 2004-01-0925.
- Rakopoulos, C.D., Rakopoulos, D.C., Giakoumis, E.G. and Kyritsis, D.C. (2004b) ‘Validation and sensitivity analysis of a two-zone diesel engine model for combustion and emissions prediction’, *Energy Conversion and Management*, Vol. 45, pp.1471–1495.
- Rezeka, S.F. and Henein, N.A. (1984) *A New Approach to Evaluate Instantaneous Friction and its Components in Internal Combustion Engines*, SAE Paper No. 840179.
- Richardson, D.E. (2000) ‘Review of power cylinder friction for diesel engines’, *Trans. ASME, J. of Engineering for Gas Turbines and Power*, Vol. 122, pp.506–519.
- Stanley, R., Taraza, D., Henein, N. and Bryzik, W. (1999) *A Simplified Model of the Piston Ring Assembly*, SAE Paper No. 1999-01-0974.
- Taraza, D., Henein, N. and Bryzik, W. (2000) *Friction Losses in Multi-cylinder Diesel Engines*, SAE Paper No. 2000-01-0921.
- Tuccillo, R., Arnone, L., Bozza, F., Nocera, R. and Senatore, A. (1993) *Experimental Correlations for Heat Release and Mechanical Losses in Turbocharged Diesel Engines*, SAE Paper No. 932459.
- Watson, N. (1981) *Transient Performance Simulation and Analysis of Turbocharged Diesel Engines*, SAE Paper No. 810338.
- Watson, N. and Marzouk, M. (1977) *A Non-linear Digital Simulation of Turbocharged Diesel Engines Under Transient Conditions*, SAE Paper No. 770123.
- Whitehouse, N.D. and Way, R.G.B. (1969–1970) ‘Rate of heat release in diesel engines and its correlation with fuel injection data’, *IMEchE – Part 3J*, Vol. 184, pp.17–27.
- Winterbone, D.E. (1986) ‘Transient performance’, in Horlock, J.H. and Winterbone, D.E. (Eds.): *The Thermodynamics and Gas Dynamics of Internal Combustion Engines*, Vol. II, Oxford: Clarendon Press, pp.1148–1212.
- Winterbone, D.E. and Tennant, D.W.H. (1981) *The Variation of Friction and Combustion Rates During Diesel Engine Transients*, SAE Paper No. 810339.
- Winterbone, D.E., Benson, R.S., Closs, G.D. and Mortimer, A.G. (1976) ‘A comparison between experimental and analytical transient test results for a turbocharged diesel engine’, *IMEchE*, Vol. 190, pp.267–276.
- Zweiri, Y.H., Whidborne, J.F. and Seneviratne, L.D. (2000) ‘Instantaneous friction components model for transient engine operation’, *Proc. Inst. Mech. Engrs – Part D: Journal of Automobile Engineering*, London, UK, Vol. 214, pp.809–824.

Note

¹In all the following Figures, engine mean oil temperature, over an engine cycle, is assumed to be 90°C unless otherwise stated.

Nomenclature

A	Surface area, m ²
A_R	Arm ratio of rocker arm
c	Radial clearance, m
C	Coefficient
d	Diameter, m
D	Cylinder bore, m
f	Friction coefficient
F	Force, N
G	Mass moment of inertia, kg m ²
h_{oil}	Oil film thickness, m
k	Thermal conductivity, W/m K
K	Stiffness, N/m or combustion model preparation rate constant
L	Length, m or lift, m
L_F	Loading force, N
m	Mass, kg
N	Engine speed, rpm
p	Pressure, bar
Q	Heat loss, J
r	Crank radius, m
s	Duty parameter
S	Thickness, m
T	Temperature, K
T_{DE}	Diametral elastic tension, N
t	Time, s
u	Velocity, m/s
V	Volume, m ³
w	Width, m
<i>Greek symbols</i>	
μ	Dynamic viscosity, N s/m ²
τ	Torque, N m
φ	Crank angle measured from the BDC position, deg
ω	Angular velocity, rad/s
<i>Subscripts</i>	
o	Initial conditions
aux	Auxiliaries
b	Bearing
cr	Critical
crod	Connecting rod
e	Engine

fr	Friction
g	Gas
inj	Injection
lp	Low pressure (pump)
L	Load
pist	Piston
pr	Piston rings
pra	Piston rings assembly
ps	Piston skirt
s	Spring
thr	Thrust
trans	Transient
w	Wall

Abbreviations

°CA	Degrees crank angle
BDC	Bottom dead centre
fmep	Friction mean effective pressure, bar
rpm	Revolutions per minute
SMD	Sauter mean diameter, μm
TDC	Top dead centre
